RSC Advances

PAPER

View Article Online
View Journal | View Issue

Check for updates

Cite this: *RSC Adv.*, 2025, **15**, 24760

Investigating the synergistic effect of defect rich V_2O_5/MWCNTs heterostructure for improved electrochemical performance of supercapacitors†

Usama Younas,[ab] Shakeel Abbas,[ac] Amina Zafar,[d] Saqib Javed,[e] Atia Khalid,[f] Shafqat Hussain,[a] Shafqat Karim,[a] Yasir Faiz,[g] Faisal Faiz,[h] Amna Safdar,[i] Amjad Nisar *[a] and Mashkoor Ahmad *[a]

The synergistic effect of V_2O_5 and multiwall carbon nanotubes (MWCNTs) offers a promising strategy to enhance the redox activity of electrode materials for high-performance supercapacitors. In this study, a simple, scalable, and cost-effective hydrothermal approach is employed to synthesize V_2O_5/MWCNTs heterostructure. The resulting heterostructure exhibits rich oxygen vacancy defects, improved conductivity, favorable structural characteristics, and abundant active sites. DFT study further demonstrate the excellent kinetics of V_2O_5/MWCNTs as compared to pristine V_2O_5 structure. Electrochemical analysis reveals that V_2O_5/MWCNTs electrode achieves good capacitance of 820 F g^{-1} at 1 A g^{-1}, significantly outperforming pristine V_2O_5 (463 F g^{-1}) in a 1.0 M neutral Na_2SO_4 solution. Moreover, the developed supercapacitor (V_2O_5/MWCNTs//AC) device shows a capacitance of 125 F g^{-1} at 1 A g^{-1}. The device also delivers an efficient energy density of 39 Wh kg^{-1} at a power density of 805 W kg^{-1}. Additionally, it exhibits outstanding cycling stability, retaining 93% of its capacity after 8000 cycles at 3 A g^{-1}. These exceptional results highlight the potential of the V_2O_5/MWCNTs heterostructure as a viable electrode material for future energy devices.

Received 14th May 2025
Accepted 7th July 2025

DOI: 10.1039/d5ra03394b

rsc.li/rsc-advances

Open Access Article. Published on 14 July 2025. Downloaded on 6/16/2026 11:11:40 AM.
This article is licensed under a Creative Commons Attribution-NonCommercial 3.0 Unported Licence.

1 Introduction

Exploring novel renewable energy sources and storage technologies is essential to meeting the growing global energy demand. Consequently, the development of high-performance, environmentally friendly renewable energy storage devices is crucial.[1] Electrochemical energy conversion and storage devices play a vital role in modern society. Among these, supercapacitors (SCs) have attracted significant attention due to their wide operating temperature range, rapid charge–discharge capabilities, and high-power density. These characteristics make them ideal for applications such as uninterruptible power systems and electric and hybrid vehicles. However, the low energy density and limited cyclic stability of SCs reduce its utilization. To resolve these issues, researchers are directing on developing advanced electrode materials to boost their performance.

The performance of supercapacitors is largely dependent on electrode material. Up till now various types of electrode materials have been explored including: carbon based[2,3] transition metal oxides (TMO)[4,5] and conducting polymers[6,7] for supercapacitor applications. Among TMO, V_2O_5 is particularly promising due to its environmental friendliness, pseudocapacitive mechanisms and high voltage range. Notably, V_2O_5 electrode participate in redox reactions through multiple oxidation states, offering several advantages, such as excellent electrochemical performance and improved device efficiency.[8] During charging, V_2O_5 undergoes oxidation, where vanadium ions lose electrons and transition to a higher oxidation state. This process results in the storage of energy in the form of chemical potential energy within the V_2O_5 structure. In recent years, defect engineering has gained attention due to its ability to enhance charge transfer and increase active sites in electrode materials. Oxygen defects significantly facilitate the creation of additional active sites and regulated migration paths for carrier ions, which effectively accelerates the electrochemical reaction kinetics and enhances electrochemical properties[9] The structural stability and electrical conductivity

[a]*Nanomaterials Research Group, Physics Division, PINSTECH, Islamabad 44000, Pakistan. E-mail: chempk@gmail.com; mashkoorahmad2003@yahoo.com*
[b]*Allama Iqbal Open University, H-8, Islamabad 44000, Pakistan*
[c]*Department of Chemistry, Government College University, Faisalabad, Pakistan*
[d]*Central Analytical Facility Division, PINSTECH, Islamabad 44000, Pakistan*
[e]*Theoretical Physics Division, PINSTECH, Islamabad 44000, Pakistan*
[f]*School of Materials Science and Engineering, Tsinghua University, Beijing, China*
[g]*Chemistry Division, PINSTECH, Islamabad 44000, Pakistan*
[h]*College of Electronics and Information Engineering, Shenzhen University, Shenzhen, PR China*
[i]*School of Chemical and Materials Engineering, National University of Science and Technology, Islamabad 44000, Pakistan*

† Electronic supplementary information (ESI) available. See DOI: https://doi.org/10.1039/d5ra03394b

© 2025 The Author(s). Published by the Royal Society of Chemistry

Open Access Article. Published on 14 July 2025. Downloaded on 6/16/2026 11:11:40 AM. This article is licensed under a Creative Commons Attribution-NonCommercial 3.0 Unported Licence.

of vanadium oxides can be significantly improved through compositional modification, leading to enhanced electrochemical performance.[10] However, V_2O_5 has some drawbacks such as limited cycling stability, insufficient electroconductivity and a low surface area.[11] In this context, scientists have been actively working to enhance its conductivity by combining with conductive materials (*e.g.* graphene, and carbon nanotube CNTs).[12,13] Multiwall carbon nanotubes (MWCNTs) known for their high conductivity, large surface area and chemical stability, are widely considered as ideal material for constructing composite structures for energy storage applications,[14,15] therefore, the combination of MWCNTs and V_2O_5 holds significant promise for enhancing the performance of energy storage devices due to their synergistic properties. The incorporation of conductive carbon materials such as MWCNTs can significantly enhance mass transfer, ion transport, and electrochemical kinetics of V_2O_5, thereby improving its overall electrochemical performance.[16] For instance, B. Saravanakumar *et al.* developed hybrid nano composite that showed a specific capacitance of 410 F g^{-1} with a capacity retention of 86.4%.[17] Similarly, B. Pandit *et al.*, synthesized V_2O_5 encapsulated MWCNTs nanostructure that exhibited good cyclic stability, maintaining with capacity retention 93% over 4000 cycles.[18] Additionally, N. Aliahmad *et al.*, synthesized V_2O_5/single-walled carbon nanotubes composites as cathode materials for high performance lithium-ion battery.[19] These studies underscore the urgent need for the development of electrode material with excellent transport features for high performance supercapacitors.

Herein, V_2O_5/MWCNTs heterostructures are synthesized by employing hydrothermal method. The synthesized V_2O_5/MWCNTs electrode attained a capacitance of 820 F g^{-1} at 1 A g^{-1}. The designed asymmetric supercapacitor device demonstrates excellent figure of merits such as: energy density of 39 Wh kg^{-1} at a power density of 805 W kg^{-1} and 93% stability over 8000 cycles, making it highly suitable for practical energy storage applications.

2 Experimental

2.1 Chemicals

Vanadium pentoxide (V_2O_5), multi-walled carbon nanotubes (MWCNTs) were purchased from Sigma Aldrich. Hydrogen peroxide solution (H_2O_2) was obtained from the Honeywell. $NaNO_3$ and $KMnO_4$ were purchased from Scharlau. Ethanol was purchased from AnalaR. Sulphuric acid (H_2SO_4) and hydrochloric acid (HCl) were purchased from MERCK.

2.2 Synthesis of V_2O_5

The synthesis of V_2O_5 was carried out as follows. In this process, 0.455 g V_2O_5 was added in 40 mL of deionized water (DI) and stirred, followed by dropwise addition of 6.25 mL of H_2O_2 with 30 minutes under stirring. The prepared solution was shifted to a 50 mL Teflon-lined autoclave and heated at 205 °C for 3 days. After cooling, the prepared product was washed three times using DI water and ethanol. The obtained product was dried at 60 °C for 6 hours. Finally, the product was annealed at 500 °C for 2 hours and ground into a fine powder.

2.3 Synthesis of V_2O_5/MWCNTs hybrid structure

The V_2O_5/MWCNTs structure was synthesized by employing a facile hydrothermal method. MWCNTs were assumed to have a weight ratio of 10% of V_2O_5. Briefly, the MWCNTs were dispersed in 20 mL of DI water and ultra-sonicated for 45 minutes. Then, 2 mL of acetic acid was added dropwise. After 10 minutes of stirring, 10 mL of the prepared solution of annealed V_2O_5 was added drop by drop to the already prepared solution. After 30 minutes of stirring at ambient temperature, the resulting solution was shifted into a Teflon-lined autoclave and placed in an oven at 200 °C for 3 h. The obtained product was filtered and washed several times with DI water and ethanol and dried at 60 °C for 6 hours.

2.4 Characterization

The synthesized products were characterized by different characterization techniques. The phase purity was analyzed by X-ray diffraction (XRD) with Cu Kα radiation ($\lambda = 1.5406$ Å). FTIR Spectrometer (Thermo Fisher Scientific Nicolet™ iS50) was employed to collect FTIR spectra. The morphology of the products was characterized by scanning electron microscopy (SEM, TESCAN MIRA, A-3) along with energy dispersive X-ray (EDS) system. The detailed structural analysis was investigated by high resolution transmission electron microscope (HRTEM, JEOL JEM-2100F, 200 kV). X-ray photoelectron spectroscopic analysis (XPS) was conducted by using ESCA-LAB 250Xi instrument using a monochromatic Al-Kα radiation source. Brunauer–Emmett–Teller (BET) specific surface area was calculated by measuring N_2 absorption–desorption isotherms. Density functional theory (DFT) study was performed to find the kinetics.

2.5 Electrochemical measurements

The constructed electrodes were evaluated by using the electrochemical workstation CHI660E in a three-electrode configuration. In this configuration, the material grown on Fluorine Tin Oxide (FTO) glass substrate as working, platinum as counter and $Hg/HgCl_2$ as a reference electrode were used. The cyclic voltammetry (CV) response was recorded in a 1.0 M Na_2SO_4 electrolyte at a scan rate between 10 to 60 mV s^{-1}. The galvanostatic charge–discharge (GCD) were measured at current densities from 1 to 5 A g^{-1}. The electrochemical impedance spectroscopy (EIS) was completed in frequency range of 0.1 Hz to 100 kHz. All the analysis was performed at room temperature. The specific capacitance of the electrodes can be find by using the following equation

$$C_s = \frac{I_d \times t_d}{\Delta V \times m} \quad (1)$$

where C_s is the specific capacitance (F g^{-1}), m is the electrode's active mass, I_d is the discharge current (A g^{-1}), ΔV is the voltage window and t_d is the discharge time period (s).

Open Access Article. Published on 14 July 2025. Downloaded on 6/16/2026 11:11:40 AM. This article is licensed under a Creative Commons Attribution-NonCommercial 3.0 Unported Licence.

2.6 Fabrication of asymmetric supercapacitor (V_2O_5/MWCNTs//AC) device

The fabrication of an asymmetric supercapacitor (V_2O_5/MWCNTs//AC) device was carried out by using V_2O_5/MWCNTs as a positive electrode and active carbon as a negative electrode, a cellulose membrane was used as separator and 1 M Na_2SO_4 as an electrolyte. The electrochemical performance of the device was performed by a two-electrode system. The mass ratio between the negative (M^-) and positive electrode (M^+) was maintained by using the charge balance ($q^+ = q^-$) equation:

$$\frac{M^+}{M^-} = \frac{C_s^- V^-}{C_s^+ V^+} \quad (2)$$

Moreover, the energy and power density of electrodes were calculated using the following equations.

$$E = \frac{C_s \times \Delta V^2}{7.2} \quad (3)$$

$$P = \frac{3600 \times E}{\Delta T} \quad (4)$$

3 Results and discussion

3.1 Structural, morphological and compositional analysis

XRD analysis was performed to analyze the phase purity as well as crystalline structure of the developed material. Fig. 1(a) reveals the XRD peaks of pristine V_2O_5 nanocrystal. All the sharp diffractions peak, centered at 2θ values 15.3°, 20.2°, 21.8°, 25.8°, 30.9°, 32.5°, 34.1°, 41.2°, 45.4°, 47.4° and 62.1° corresponding to the (200), (001), (101), (110), (301), (011), (310), (200), (411), (302), and (710) crystal planes. These peaks align well with V_2O_5 according to (JCPDS no. 41-1426). In addition, the heterostructure pattern shows abroad peak (marked with *) at 25.8° and a weak peak at 43.2° corresponds to (002) and (100) planes of MWCNTs. Moreover, the intensity of peak at 25.8° in V_2O_5/MWCNTs pattern is higher as compared to pristine V_2O_5 structure which further confirms the successful formation of V_2O_5/MWCNTs heterostructure.

Fig. 1(b) displays the Raman spectra of pristine V_2O_5 and V_2O_5/MWCNTs heterostructure. The resulted spectra display peaks at 145, 195, 283, 407, 693, 995 cm^{-1}, which indicates the presence of V_2O_5 heterostructure. The peaks at 145 and 195 cm^{-1} are ascribed to the chain translation which is associated with the layered structure.[20] Two peaks at 283 and 407 cm^{-1} are associated to V=O bonds of bending and stretching vibrations.[21] The Raman peaks appeared at 693 and 995 cm^{-1} describe the stretching modes of bridging of oxygen (V_2–O) and terminal oxygen (V=O), respectively. Besides, two prominent peaks at 1471 and 1587 cm^{-1} also appear which are related to the D and G band of MWCNTs.[22] The D bands signify the degree of defects and G band related to the stretching vibration of C–C bond as well as the vibration of sp^2 bonded carbon atoms. It is observed that the intensity ratio of the D to G band (ID/IG) in V_2O_5/MWCNTs (1.02) is larger than MWCNTs (0.95), representing that the surface of V_2O_5/MWCNTs is rough and has many defects. The Raman spectrum of MWCNTs is also presented in Fig. S1.†

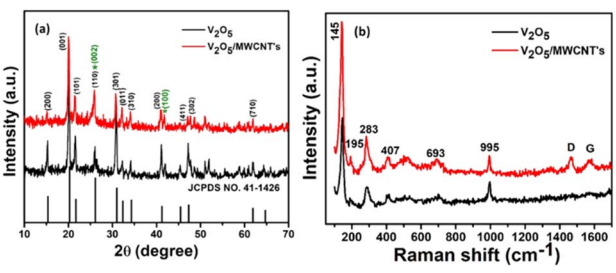

Fig. 1 (a) XRD pattern and (b) Raman spectra of V_2O_5 and V_2O_5/MWCNT's.

Fig. 2(a) presents the SEM image of the V_2O_5 structure, revealing that the product consists of a large number of nanocrystals. Fig. 2(b) displays the SEM image of the V_2O_5/MWCNTs heterostructure, where V_2O_5 nanocrystals are observed to functionalize the MWCNTs, forming a heterostructure. Fig. 2(c) shows the EDX spectrum of the V_2O_5/MWCNTs heterostructure, confirming the presence of V, C, and O elements, which indicates successful heterostructure formation. Furthermore, the detailed structure of both materials was investigated using TEM and HRTEM. Fig. 2(d) presents the TEM image of the V_2O_5/MWCNTs heterostructure, demonstrating that the V_2O_5 nanocrystals are strongly bonded to the MWCNTs, further supporting the SEM observations. Fig. 2(e) and (f) show HRTEM images of the V_2O_5/MWCNTs heterostructure, captured from different areas of Fig. 2(d). The measured lattice fringes of the heterostructure are approximately ~0.35 nm, corresponding to the (110) plane of V_2O_5. Additionally, the presence of multiple fringes confirms the multilayer structure of MWCNTs. Additionally, the SEM images of pure MWCNTs and V_2O_5 NPs along with EDX is also shown in Fig. S2(a)–(c).†

To examine the specific surface area of the synthesized material BET was performed. Fig. S3.† displays the nitrogen adsorption–desorption isotherms of the V_2O_5 and V_2O_5/

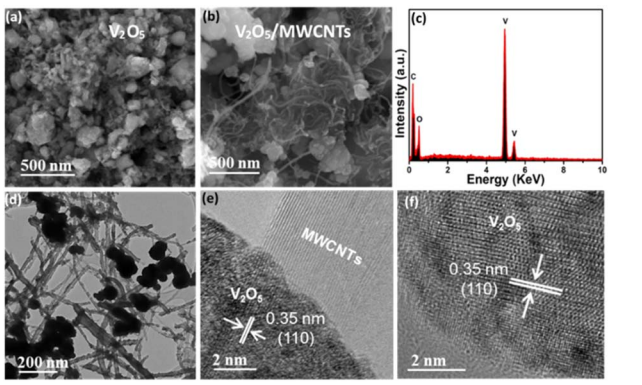

Fig. 2 SEM images of (a) V_2O_5 (b) V_2O_5/MWCNTs (c) EDX spectrum of V_2O_5/MWCNTs (d) TEM and (e and f) HRTEM images of V_2O_5/MWCNTs taken from (d).

© 2025 The Author(s). Published by the Royal Society of Chemistry

Open Access Article. Published on 14 July 2025. Downloaded on 6/16/2026 11:11:40 AM. This article is licensed under a Creative Commons Attribution-NonCommercial 3.0 Unported Licence.

MWCNTs heterostructure obtained at 77 K. Its isotherms curves demonstrate that heterostructure material exhibits enhanced specific surface area (110 $cm^2 g^{-1}$) as compared to pristine V_2O_5 (81 $cm^2 g^{-1}$). The increased in heterostructure surface area is attributed to the incorporation of MWCNTs. The improved surface area facilitates better interaction between electrode material and electrolyte ions, improved charge transfers and ultimately leading to higher specific capacitance.

Fig. S4(a)† shows the XPS survey spectrum of V_2O_5/MWCNTs heterostructure. The existence of vanadium, oxygen, and carbon elements confirm the formation of heterostructure. Fig. 3(a) displays the de-convoluted high-resolution spectrum of V 2p peak, indicating mixed valence states of vanadium oxide. The spectrum consists of two major peaks observed at 517.5 and 524.8 eV correspond to V $2p_{3/2}$ and V $2p_{1/2}$ electronic states respectively.[23] Both V $2p_{1/2}$ and V $2p_{3/2}$. Regions are composed of V^{5+} and V^{4+} states located at specific binding energies. The strong interfacial interaction in heterostructure facilitate electron transfer from MWCNTs to V_2O_5. The presence of strong V^{4+} state indicates the reduction of V^{5+} to V^{4+} which is closely associated with the formation of oxygen vacancies.[24] Moreover, the electron transfer also introduces some localized strain or defects at the interface, which can further encourage defect formation in the V_2O_5 lattice. In addition, close observation shows that V 2p peak in heterostructure reveals a small shift as compared to pristine V 2p peak (Fig. S4b†) which further indicate the generation of defects. Fig. 3(b) shows the deconvoluted C 1s which splits into three peaks. The main peak at 284.2 eV corresponds to C–C bond (sp^2). The additional peak at 284.4 eV recognized to C–O and 285.6 eV to O–C=O. The presence of these peaks shows the formation of covalent bond between MWCNTs and V_2O_5. Fig. 3(c) and (d) reveals the deconvoluted spectrum of O 1s peak for both structures. The heterostructure spectrum exhibits two binding energy peaks located at 529.6 and 533.3 eV. The peak at 529.6 eV belongs to M–O bond in V_2O_5 structure while at 533.3 eV corresponds to the oxygen deficient region due to oxygen vacancies (OV) caused by the ability of V_2O_5 to accommodate changes in valence states. The comparison of intensity ratios (O_V/O_L) of V_2O_5/MWCNTs (0.42) and V_2O_5 (0.36) demonstrates the increased amount of oxygen vacancy defects in the heterostructure. The XPS results are in good agreement with the Raman findings.

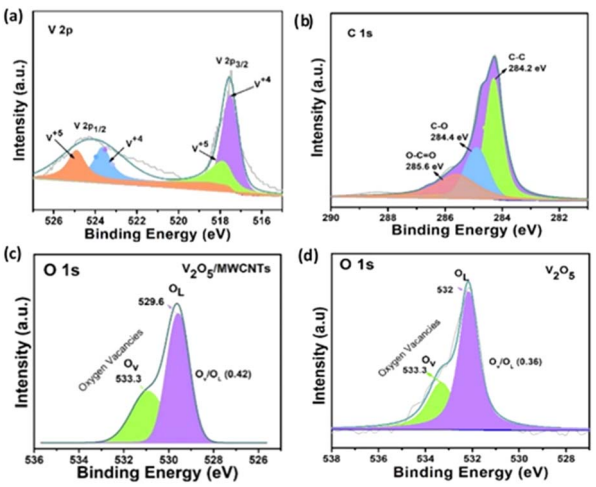

Fig. 3 XPS spectrum of (a) V 2p (b) C 1s (c) O 1s spectrum of V_2O_5/MWCNTs heterostructure (d) O 1s spectrum of V_2O_5 nanostructure.

FTIR spectra of V_2O_5 and V_2O_5/MWCNTs heterostructures are recorded to investigate the functional groups. Fig. S5† presents the FTIR spectrum performed from 3500–400 cm^{-1}. It can be seen that spectra consist of peaks located at 1916, 991, 770, 637, 481, 445 cm^{-1}. The band at 445 cm^{-1} belongs to the triply coordinated oxygen atom between three vanadium atoms. The band located at 481 cm^{-1} assigned to the vanadyl stretching mode (δ_{V-O}). The peak at 637 cm^{-1} corresponds to asymmetric and symmetric stretching of V–O–V bridge. Sharp peaks at 770 and 991 cm^{-1} indicate the metal oxide bond which confirms successful formation of V_2O_5/MWCNTs heterostructures.

3.2 Super capacitive performance of V_2O_5/MWCNT's electrodes

In order to evaluate the best performance of V_2O_5/MWCNTs electrode, the electrode was tested in 1 M KOH, NaOH and Na_2SO_4 electrolyte. It was observed that Na_2SO_4 provided a wider potential window than other electrolytes as shown in Fig. S6.† Based on these results, Na_2SO_4 was selected to achieve a higher energy density. Cyclic voltammetry (CV) is a versatile and widely used electrochemical technique that provides valuable information about the electrochemical behaviour of the materials. Fig. 4(a) illustrates the comparative analysis of CV response of V_2O_5 and V_2O_5/MWCNTs electrodes at a scan rate of 20 mV s^{-1}. The CV curves show quasi-rectangular shape with redox couple further confirm the excellent pseudo-capacitive behaviour and good reversibility. It can be observed that the area under the curve of V_2O_5/MWCNTs electrode is larger than V_2O_5 electrode, which shows that MWCNTs expressively improved the electrochemical behaviour of V_2O_5. Fig. 4(b) shows the CV response of V_2O_5/MWCNTs electrode at potential −0.4 to 1.0 V with scan rates from 10 to 60 mV s^{-1}. It is clearly observed that integral area of the CV curves increases with the increase in scan rates. Moreover, the shape of the curves remains similar, which confirm the good stability of the electrode. The surface-controlled (capacitive) and diffusion-controlled contributions of the electrode material were evaluated using Dunn's method, based on the power-law relationship.

$$i = av^b \quad (5)$$

$$\log(i) = \log(a) + b\log(v) \quad (6)$$

The constant parameter "a" the slope "b" can be determined by $\log v$–$\log i$ correlation as shown in Fig. 4(c). The values of b are calculated to be 0.88 and 0.92 corresponded with peaks A and B. It is observed that the value of "b" approaching 1.0, which indicates the dominancy of capacitive kinetics for energy storage process of V_2O_5/MWCNTs electrode. Moreover, the capacitive and diffusion contributions ratio is also investigated.

© 2025 The Author(s). Published by the Royal Society of Chemistry

Open Access Article. Published on 14 July 2025. Downloaded on 6/16/2026 11:11:40 AM. This article is licensed under a Creative Commons Attribution-NonCommercial 3.0 Unported Licence.

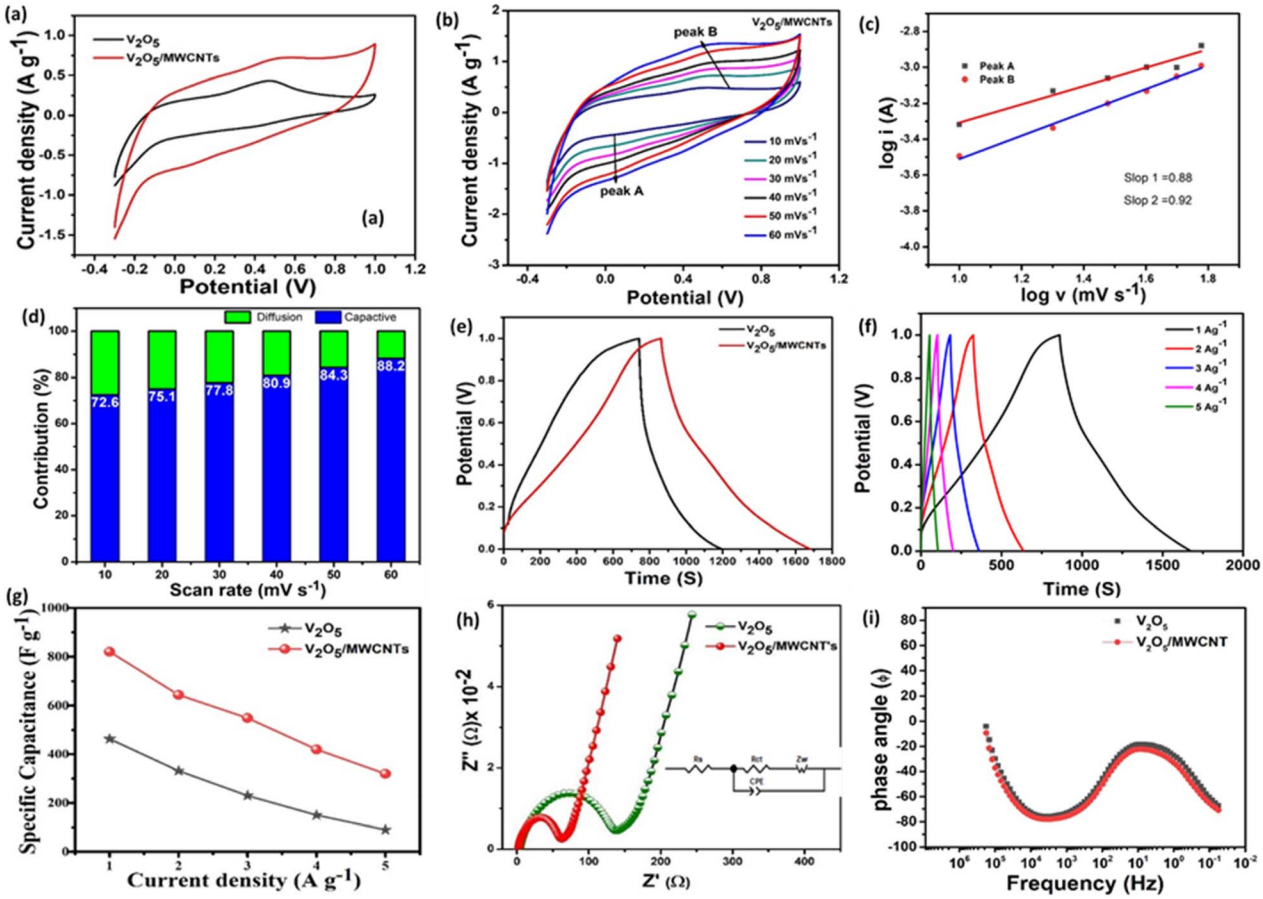

Fig. 4 (a) Comparative CV curves of V_2O_5 and V_2O_5/MWCNTs electrodes at 20 mV s^{-1} (b) CV curve of V_2O_5/MWCNTs at various scan rates (c) plot of log *v vs.* log *i* (d) ratios of diffusion and capacitive contributions (e) comparative GCD curves of V_2O_5 and V_2O_5/MWCNTs electrodes at 1 A g^{-1} (f) GCD curves of V_2O_5/MWCNTs electrode at different current densities (g) specific capacitance *vs.* current densities of V_2O_5 and V_2O_5/MWCNTs electrodes (h) Nyquist plots of V_2O_5 and V_2O_5/MWCNT's electrodes; inset is the AC equivalent circuit model (i) Bode phase angle plot.

The current response at a given potential $i(V)$ can be categorized as diffusion-controlled process ($K_2v^{1/2}$) and capacitive contribution (K_1v). These categorized are possible using the eqn (7) and (8):

$$i(V) = K_1v + K_2v^{1/2} \quad (7)$$

Eqn (7) can be further transformed into:

$$\frac{i(V)}{v^{1/2}} = K_1v^{1/2} + K_2 \quad (8)$$

where K_1 and K_2 are changeable coefficients, which can be extracted based on the relation between $v^{1/2}$ and $i(V)/v^{1/2}$. The capacitive and diffusion contribution ratio of V_2O_5/MWCNTs electrode is shown in Fig. 4(d). It is important to note that, the capacitive contribution is raised from 72.6% to 88.2% with the increase in scan rate from 10 to 60 mV s^{-1}. It is evident that, at lower scan rate, diffusion-controlled charge storage may increase due to sufficient time for the interaction of the electrolyte with all the active sites of the electrode and at high scan rate the capacitive behaviour is clearly predominant over diffusion contribution. Due to these results V_2O_5/MWCNTs is a suitable electrode to explore the electrochemical redox reactions phenomenon.

Galvanostatic charge–discharge (GCD) is also used to measure the charge and discharge behavior of the electrode. Fig. 4(e) shows the comparative GCD curves of pristine V_2O_5 and heterostructure V_2O_5/MWCNTs electrodes at 1 A g^{-1}. As observed, the heterostructure has a long discharge time than that of pristine V_2O_5 electrode. Fig. 4(f) illustrates the GCD profile of V_2O_5/MWCNTs electrode at current densities in the range of 1 to 5 A g^{-1}. Fig. 4(g) presents the specific capacitance calculated from GCD curves at different current densities. It is worth noting that, the V_2O_5/MWCNTs electrode achieved the improved capacitance of ~820 F g^{-1} at 1 A g^{-1}. The GCD behavior of pristine V_2O_5 electrode is also performed at different current densities in the range of 1 to 5 A g^{-1} as shown in Fig. S7.† The cyclic stability of V_2O_5 and V_2O_5/MWCNTs electrodes at 2 A g^{-1} is also evaluated as shown in Fig. S8.† It can be observed that the heterostructure electrode exhibits outstanding cyclic stability up to 8000 cycles with a capacity retention of 94%, better than V_2O_5 electrode. The results demonstrate that V_2O_5/MWCNTs electrode has a superior

© 2025 The Author(s). Published by the Royal Society of Chemistry

Open Access Article. Published on 14 July 2025. Downloaded on 6/16/2026 11:11:40 AM. This article is licensed under a Creative Commons Attribution-NonCommercial 3.0 Unported Licence.

Table 1 Electrochemical performance comparison of fabricated V_2O_5/MWCNTs electrode and reported V_2O_5 based electrodes

Material	Specific capacitance ($F\ g^{-1}$)	Current density ($A\ g^{-1}$)	Energy density ($Wh\ kg^{-1}$)	Cyclic stability (%)	Cycle numbers	References
Carbon coated V_2O_5	417	0.5	10.3	92	2000	26
V_2O_5/MWCNTs	629	2	72	96	4000	27
V_2O_5/MWCNTs core/shell hybrid aerogels	625	0.5	86.8	—	20 000	28
C@V_2O_5 nanorods	417	0.5	9.4	76	1000	29
V_2O_5/CNTs–SAC	357.5	10	—	99.5	1000	30
C-dot@V_2O_5	270	1	60	87	5000	31
W-doped V_2O_5	407	0.5	246	—	—	32
V_2O_5/rGO	484	0.5	7.4	83	1000	33
V_2O_5@rGO	574.5	1	46.05	82.7	5000	34
V_2O_5/MWCNTs	410	0.5	57	86	600	35
V_2O_5/MWCNTs	**820**	**1**	**39**	**93**	**8000**	**This work**

performance as compared to V_2O_5 electrode as well as previously reported work shown in and Table 1.

EIS is also performed to evaluate the charge kinetics of the electrodes. Fig. 4(h) shows comparative Nyquist plots of electrodes measured in 1.0 M Na_2SO_4 electrolyte. The high-frequency intercept on the real axis represents the bulk resistance (R_s) of the electrode and electrolyte. A depressed semicircle in the mid-frequency region reflects the combined effects of charge transfer resistance (R_{ct}) and double-layer capacitance (CPE electrode). The experimental data is fitted using an equivalent circuit model as shown in the inset Fig. 4(f). In the equivalent circuit model, a constant phase element (CPE) is used to account for non-ideal capacitive behaviour. The low-frequency region approximately at 45°, corresponding to the Warburg impedance (W). The semicircle diameter of the Nyquist plots shows the charge transfer resistance between electrolyte and electrode. The small semicircle of V_2O_5/MWCNTs electrode demonstrates low charge transfer resistance (R_{ct}) of 62.3 Ω. The fitting parameters of electrodes are presented in the Table S1 (ESI†). The improved kinetics of V_2O_5/MWCNTs electrode is the results of synergy between V_2O_5 and MWCNTs.

Fig. 4(i) presents the Bode phase angle plot to provide a comprehensive understanding of the electrochemical behaviour of the system. The Bode phase angle plot, in particular, offers critical insights that complement the Nyquist plot in evaluating electrode kinetics. The arrow indicates the direction of increasing frequency. At high frequencies, the phase angle approaches 0° indicating predominantly resistive behaviour, which is typically associated with the solution resistance (R_s) as represented in the equivalent circuit model. At intermediate frequencies, a significant phase shift (*e.g.*, toward −45° to −90°) reflects capacitive behaviour. This is commonly attributed to the double-layer capacitance in conjunction with the charge transfer resistance which is in agreement with equivalent circuit model. At low frequencies, the phase angle continues to decrease. However, due to the instrument's limitations at very low frequencies, it anticipates that the phase angle would drop below −90°. This trend is characteristic of diffusion-controlled processes and indicative of Warburg impedance. Such behaviour reflects mass transport limitations, such as ion diffusion through the electrolyte or within a porous electrode structure.

3.3 DFT calculation

To understand the superior electrochemical performance of V_2O_5/MWCNT electrode as compared to that of pristine V_2O_5, we refer to recent hybrid DFT calculations on V_2O_5/MWCNT heterostructure.[25] Specifically, it is shown that work function of MWCNT (4.22 eV) is much lower than the electron affinity of V_2O_5 (110) surface (6.40 eV). Such energy level alignment leads to a charge transfer from MWCNT to V_2O_5. This interfacial charge transfer not only increases the electron density of V_2O_5 within heterostructure but also increases its conductivity since electrons are transferred to otherwise empty conduction bands. We note further that MWCNT is itself metallic in nature. Thus, inclusion of MWCNT within heterostructure will also improve the electronic conductivity of the electrode. Considering the fact that a higher electronic conductivity of electrode promotes redox reaction kinetics; it is evident that V_2O_5/MWCNTs will have better electrochemical performance as compared to pristine V_2O_5. This is indeed confirmed by the impedance experiments (Fig. 4(f)) where V_2O_5/MWCNTs electrode has much lower charge transfer resistance as compared to pristine V_2O_5, highlighting superior redox reaction kinetic of V_2O_5/MWCNTs electrode. It is further noted that the inclusion of MWCNTs also provides additional active sites for fast charge transportation. This helps to explain enhanced specific capacitance of V_2O_5/MWCNT electrode in comparison to pristine V_2O_5.

3.4 The performance of the asymmetric prototype supercapacitor (V_2O_5/MWCNTs//AC) device

The practical feasibility of V_2O_5/MWCNTs material is evaluated by constructing a prototype asymmetric supercapacitor. In this fabrication, the V_2O_5/MWCNTs electrode used as cathode, activated carbon (AC) as an anode and Na_2SO_4 electrolyte as illustrated in Fig. 5(a).

The CV of the assembled ASC device at voltages from 0 to 1.5 V is shown in Fig. 5(b). As observed, the device can operate in a wide voltage window. Fig. 5(c) illustrates the CV response of the device at various scan rates in the range from 10 to 50 mV s^{-1}. It can be seen that the increase in scan rates has no effect the shape of the CV curves and kept similar shape, represent the fast oxidation/reduction reactions with good rate capability.

Open Access Article. Published on 14 July 2025. Downloaded on 6/16/2026 11:11:40 AM.
This article is licensed under a Creative Commons Attribution-NonCommercial 3.0 Unported Licence.

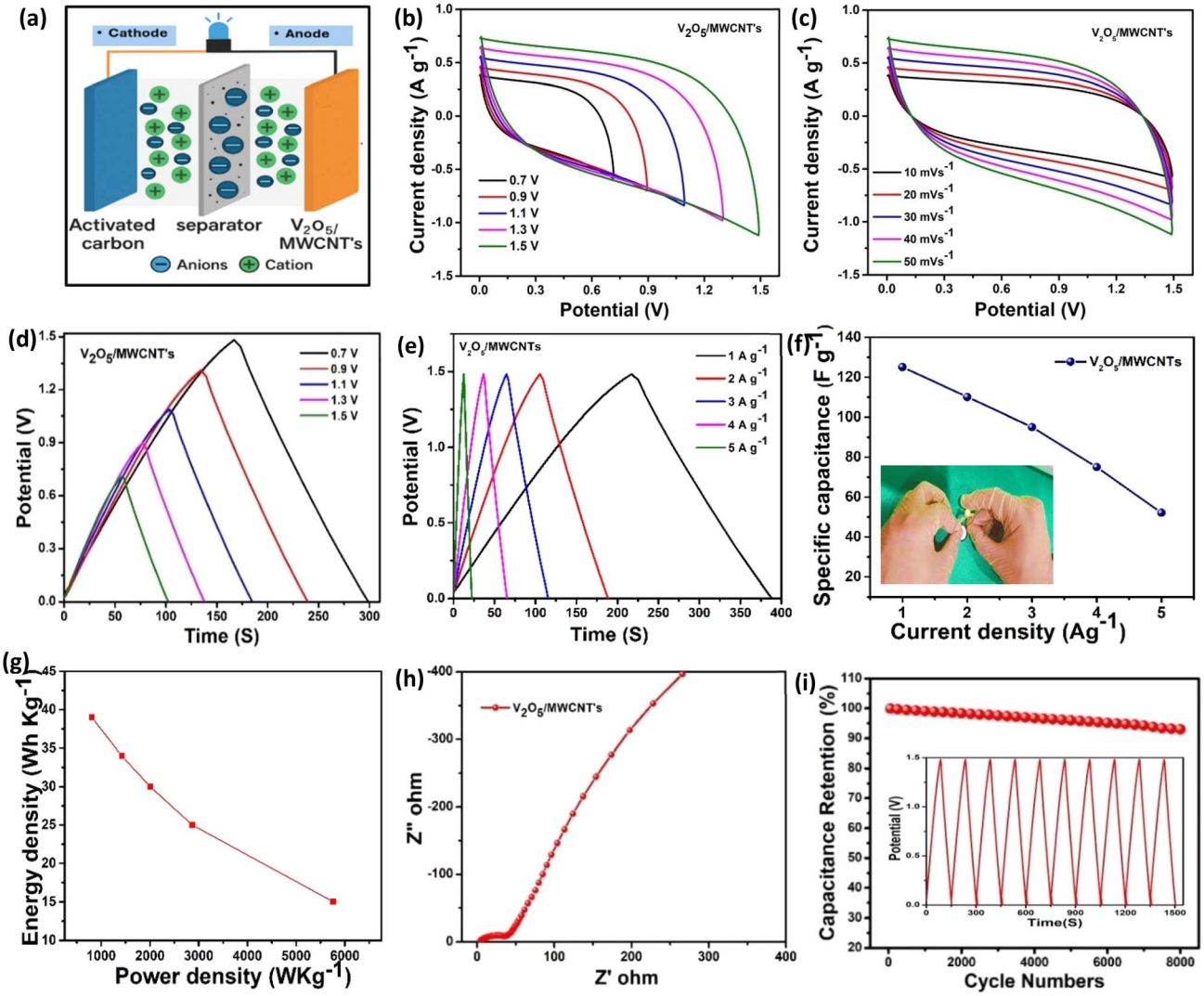

Fig. 5 (a) Schematic illustration of V_2O_5/MWCNTs//AC device (b) CV curves at various voltage windows at 50 mV s^{-1} (c) CV curves at scan rates from 10 to 50 mV s^{-1} (d) GCD curves at 1 A g^{-1} for various voltage windows (e) GCD *vs.* current densities plot (f) specific capacitance *vs.* current densities; inset shows the digital photo of the fabricated device (g) Ragone plot of device (h) Nyquist plot (i) cyclic performance of the device at 4 A g^{-1}; inset shows the GCD curves of the first 10 cycles.

Fig. 5(d) shows the GCD behaviour of the device at different voltage windows ranging from 0 to 1.5 V. Fig. 5(e) presents the GCD behaviour at different current densities in the range from 1 to 5 A g^{-1}. The triangular shape indicates the good reversibility of the device. Fig. 5(f) demonstrates the plot between capacitance *vs.* current densities. As clearly seen that the device obtained the highest capacitance of 125 F g^{-1} at 1 A g^{-1}. Moreover, the practical feasibility of the device is also recorded by real time LED operation, as shown in the inset Fig. 5(f). The Ragone graph of ASC device is demonstrated in Fig. 5(g). As shown the fabricated device has improved performance as compared to previously reported V_2O_5 supercapacitor devices, such as, carbon coated V_2O_5 (10.3 Wh kg^{-1}) V_2O_5/rGO (7.4 Wh kg^{-1}) V_2O_5/graphene (32.9 Wh kg^{-1})[36] respectively. Fig. 5(h) displays the Nyquist plot of the assembled device and demonstrates enhanced kinetics. Fig. 5(i) shows the cyclic stability of the device evaluated by GCD curves. The developed device shows good stability, with capacity retention of ~93% for 8000 cycles.

4 Conclusions

The V_2O_5/MWCNTs heterostructures were synthesized using a simple and cost-effective hydrothermal method. The incorporation of MWCNTs not only enhances conductivity and chemical kinetics but also mitigates electrode cracking during rapid charge–discharge cycles. Additionally, rich oxygen vacancy defects and abundant active sites facilitate efficient electrolyte ion diffusion, further improving electrochemical performance. The heterostructure is found to be promising candidate for supercapacitors, exhibiting an impressive capacitance of 820 F g^{-1} at 1 A g^{-1}, significantly surpassing that of pristine V_2O_5. Moreover, the V_2O_5/MWCNTs electrode demonstrates excellent rate capability and long-term stability. The

© 2025 The Author(s). Published by the Royal Society of Chemistry

Open Access Article. Published on 14 July 2025. Downloaded on 6/16/2026 11:11:40 AM. This article is licensed under a Creative Commons Attribution-NonCommercial 3.0 Unported Licence.

fabricated asymmetric supercapacitor (V_2O_5/MWCNTs//AC) device achieves an energy density of 39 Wh kg^{-1} with capacity retention of 93% for 8000 cycles at 3 A g^{-1}. These outstanding properties propose that V_2O_5/MWCNTs heterostructure is a highly promising electrode material for supercapacitors. This approach can also be extended to develop various heterostructures for next-generation energy storage devices.

Data availability

The authors confirm that the data supporting the findings of this study are available within the article and its ESI.†

Author contributions

M. A. proposed the idea. U. Y. and S. A. performed the experiment and prepared the materials. S. H. and S. K. performed the Raman measurements. A. Z., and Y. F. analyzed the materials by using XRD and SEM. A. K. and F. F. carried out the TEM and HRTEM. S. J. performed the DFT study. A. N. and A. S. analyzed the XPS data. U. Y. and M. A. performed electrochemical measurements and analyzed EIS. U. Y. and M. A. co-wrote the whole article. The whole research work was supervised by M. A. and A. N.

Conflicts of interest

The authors declare no conflict of interest.

Acknowledgements

This work was supported by Pakistan Atomic Energy Commission (PAEC). The authors are thankful to ICTP for funding under the ICTP-Elettra users' program. All authors also thank the helps of Mr Muhammad Hussain, Materials Division, PINSTECH for XRD data collection.

References

1 T.-Z. Ang, M. Salem, M. Kamarol, H. S. Das, M. A. Nazari and N. Prabaharan, A comprehensive study of renewable energy sources: Classifications, challenges and suggestions, *Energy Strategy Rev.*, 2022, **43**, 100939.
2 M. Majumder, R. B. Choudhary and A. K. Thakur, Hemispherical nitrogen-doped carbon spheres integrated with polyindole as high performance electrode material for supercapacitor applications, *Carbon*, 2019, **142**, 650–661.
3 R. Nasser, G.-F. Zhang, H. Liang, N.-N. Zhou and J.-M. Song, Lamellar hierarchically porous carbon derived from discarded Barbary figs husk: Preparation, characterization, and its excellent capacitive properties, *J. Electroanal. Chem.*, 2021, **888**, 114930.
4 U. Banik, M. T. U. Malik, S. M. S. M. Rahat and A. K. Mallik, Performance enhancement of ruthenium-based supercapacitors: A review, *Energy Storage*, 2023, **5**, e380.
5 J. M. Xu, A. L. Yan, X. C. Wang, B. Q. Wang and J. P. Cheng, A review of cobalt monoxide and its composites for supercapacitors, *Ceram. Int.*, 2021, **47**, 22229–22239.
6 S. Sharma and P. Chand, Supercapacitor and electrochemical techniques: A brief review, *Results Chem.*, 2023, **5**, 100885.
7 N. S. Shaikh, S. B. Ubale, V. J. Mane, J. S. Shaikh, V. C. Lokhande, S. Praserthdam, C. D. Lokhande and P. Kanjanaboos, Novel electrodes for supercapacitor: Conducting polymers, metal oxides, chalcogenides, carbides, nitrides, MXenes, and their composites with graphene, *J. Alloys Compd.*, 2022, **893**, 161998.
8 C. V. V. M. Gopi, S. Alzahmi, M. Y. Al-Haik, Y. A. Kumar, F. Hamed, Y. Haik and I. M. Obaidat, Recent advances in pseudocapacitive electrode materials for high energy density aqueous supercapacitors: Combining transition metal oxides with carbon nanomaterials, *Mater. Today Sustain.*, 2024, **28**, 100981.
9 Y. Zhang, Z. Zhou, X. Tan, Y. Liu, F. Zhang, C. Meng and X. Zhu, Tailoring electronic structure to enhance the ammonium-ion storage properties of VO_2 by molybdenum doping toward highly efficient aqueous ammonium-ion batteries, *Inorg. Chem. Front.*, 2025, **12**, 355–368.
10 X. Tan, F. Zhang, D. Chen, P. Wang, Y. Liu, C. Meng and Y. Zhang, Modulating NH4+ in vanadium oxide framework for high-efficient aqueous NH4+ storage, *Chem. Eng. J.*, 2024, **489**, 151119.
11 H. Gamal, A. M. Elshahawy, S. S. Medany, M. A. Hefnawy and M. S. Shalaby, Recent advances of vanadium oxides and their derivatives in supercapacitor applications: A comprehensive review, *J. Energy Storage*, 2024, **76**, 109788.
12 M. Ramachandrarao, S. H. Khan and K. Abdullah, Carbon nanotubes and nanofibers – reinforcement to carbon fiber composites - synthesis, characterizations and applications: A review, *Compos., Part C: Open Access*, 2025, **16**, 100551.
13 A. V. Shchegolkov, A. V. Shchegolkov, V. V. Kaminskii, P. Iturralde and M. A. Chumak, Advances in Electrically and Thermally Conductive Functional Nanocomposites Based on Carbon Nanotubes, *Polymers*, 2024, **17**, 71.
14 W. Peng, Z. Su, J. Wang, S. Li, K. Chen, N. Song, S. Luo and A. Xie, MnCoOx-multi-walled carbon nanotubes composite with ultra-high specific capacitance for supercapacitors, *J. Energy Storage*, 2022, **51**, 104519.
15 B. Freitas, W. G. Nunes, D. M. Soares, F. C. Rufino, C. M. Moreira, L. M. Da Silva and H. Zanin, Robust, flexible, freestanding and high surface area activated carbon and multi-walled carbon nanotubes composite material with outstanding electrode properties for aqueous-based supercapacitors, *Materials Advances*, 2021, **2**, 4264–4276.
16 X. Tan, F. Zhang, D. Chen, J. Gong, J. Sun, C. Meng and Y. Zhang, One-step hydrothermal synthesis of vanadium dioxide/carbon core–shell composite with improved ammonium ion storage for aqueous ammonium-ion battery, *J. Colloid Interface Sci.*, 2024, **669**, 2–13.
17 B. Saravanakumar, K. K. Purushothaman and G. Muralidharan, V_2 O_5/functionalized MWCNT hybrid

Open Access Article. Published on 14 July 2025. Downloaded on 6/16/2026 11:11:40 AM. This article is licensed under a Creative Commons Attribution-NonCommercial 3.0 Unported Licence.

nanocomposite: the fabrication and its enhanced supercapacitive performance, *RSC Adv.*, 2014, **4**, 37437–37445.

18 B. Pandit, D. P. Dubal, P. Gómez-Romero, B. B. Kale and B. R. Sankapal, V2O5 encapsulated MWCNTs in 2D surface architecture: Complete solid-state bendable highly stabilized energy efficient supercapacitor device, *Sci. Rep.*, 2017, **7**, 43430.

19 N. Aliahmad, P. K. Biswas, H. Dalir and M. Agarwal, Synthesis of V2O5/Single-Walled Carbon Nanotubes Integrated into Nanostructured Composites as Cathode Materials in High Performance Lithium-Ion Batteries, *Energies*, 2022, **15**, 552.

20 I. Shafiq, M. Hussain, S. Shafique, P. Akhter, A. Ahmed, R. S. Ashraf, M. Ali Khan, B.-H. Jeon and Y.-K. Park, Systematic Assessment of Visible-Light-Driven Microspherical V2O5 Photocatalyst for the Removal of Hazardous Organosulfur Compounds from Diesel, *Nanomaterials*, 2021, **11**, 2908.

21 Q. Wei, Z. Jiang, S. Tan, Q. Li, L. Huang, M. Yan, L. Zhou, Q. An and L. Mai, Lattice Breathing Inhibited Layered Vanadium Oxide Ultrathin Nanobelts for Enhanced Sodium Storage, *ACS Appl. Mater. Interfaces*, 2015, **7**, 18211–18217.

22 C. Wang, L. Hu, Y. Hu, Y. Ren, X. Chen, B. Yue and H. He, Direct hydroxylation of benzene to phenol over metal oxide supported graphene oxide catalysts, *Catal. Commun.*, 2015, **68**, 1–5.

23 J. Jyothibasu, M.-Z. Chen, Y.-C. Tien, C.-C. Kuo, E.-C. Chen, Y.-C. Lin, T.-C. Chiang and R.-H. Lee, V2O5/Carbon Nanotube/Polypyrrole Based Freestanding Negative Electrodes for High-Performance Supercapacitors, *Catalysts*, 2021, **11**, 980.

24 Y. Sun, Z. Xie and Y. Li, Enhanced lithium storage performance of V_2O_5 with oxygen vacancy, *RSC Adv.*, 2018, **8**, 39371–39376.

25 H. Mustafa, Y. Yu, A. Zafar, Y. Liu, S. Karim, S. Javed, S. Mehboob, H. Sun, S. Hussain, A. U. Shah, S. Z. Hussain, A. Safdar, A. Nisar and M. Ahmad, MWCNT synergy for boosting the electrochemical kinetics of V_2O_5 cathode for lithium-ion batteries, *New J. Chem.*, 2022, **46**, 3417–3425.

26 S. Balasubramanian and K. K. Purushothaman, Carbon Coated Flowery V2O5 Nanostructure as Novel Electrode Material for High Performance Supercapacitors, *Electrochim. Acta*, 2015, **186**, 285–291.

27 B. Pandit, D. P. Dubal, P. Gómez-Romero, B. B. Kale and B. R. Sankapal, V2O5 encapsulated MWCNTs in 2D surface architecture: Complete solid-state bendable highly stabilized energy efficient supercapacitor device, *Sci. Rep.*, 2017, **7**, 43430.

28 Y. Wu, G. Gao, H. Yang, W. Bi, X. Liang, Y. Zhang, G. Zhang and G. Wu, Controlled synthesis of V_2O_5/MWCNT core/shell hybrid aerogels through a mixed growth and self-assembly methodology for supercapacitors with high capacitance and ultralong cycle life, *J. Mater. Chem. A*, 2015, **3**, 15692–15699.

29 B. Saravanakumar, K. K. Purushothaman and G. Muralidharan, High performance supercapacitor based on carbon coated V2O5 nanorods, *J. Electroanal. Chem.*, 2015, **758**, 111–116.

30 Q. Wang, Y. Zou, C. Xiang, H. Chu, H. Zhang, F. Xu, L. Sun and C. Tang, High-performance supercapacitor based on V2O5/carbon nanotubes-super activated carbon ternary composite, *Ceram. Int.*, 2016, **42**, 12129–12135.

31 R. Narayanan, Single step hydrothermal synthesis of carbon nanodot decorated V2O5 nanobelts as hybrid conducting material for supercapacitor application, *J. Solid State Chem.*, 2017, **253**, 103–112.

32 J. Zheng, Y. Zhang, X. Jing, Q. Wang, T. Hu, N. Xing and C. Meng, Improvement of the specific capacitance of V2O5 nanobelts as supercapacitor electrode by tungsten doping, *Mater. Chem. Phys.*, 2017, **186**, 5–10.

33 B. Saravanakumar, K. K. Purushothaman and G. Muralidharan, Fabrication of two-dimensional reduced graphene oxide supported V 2 O 5 networks and their application in supercapacitors, *Mater. Chem. Phys.*, 2016, **170**, 266–275.

34 B. Hu, C. Guo, C. Xu, Y. Cen, J. Hu, Y. Li, S. Yang, Y. Liu, D. Yu and C. Chen, Rational Construction of V $_2$ O $_5$ @rGO with Enhanced Pseudocapacitive Storage for High-Performance Flexible Energy Storage Device, *ChemElectroChem*, 2019, **6**, 5845–5855.

35 B. Saravanakumar, K. K. Purushothaman and G. Muralidharan, V_2O_5/functionalized MWCNT hybrid nanocomposite: the fabrication and its enhanced supercapacitive performance, *RSC Adv.*, 2014, **4**, 37437–37445.

36 M. Fu, Q. Zhuang, Z. Zhu, Z. Zhang, W. Chen, Q. Liu and H. Yu, Facile synthesis of V2O5/graphene composites as advanced electrode materials in supercapacitors, *J. Alloys Compd.*, 2021, **862**, 158006.

© 2025 The Author(s). Published by the Royal Society of Chemistry